Retrospective Cohort Study

INTERNATIONAL JOURNAL OF SURGERY

OPEN

Development and validation of a CT-based radiomics model to predict survival-graded fibrosis in pancreatic ductal adenocarcinoma

Siya Shi, MD[a], Ruihao Liu, MS[c,d,h], Jian Zhou, MD[b,e], Jiawei Liu, MD[a], Hongxin Lin, MS[c,d], Junyang Mo, MS[c,d], Jian Zhang, PhD[f,g], Xianfen Diao, PhD[c,d,h], Yanji Luo, MD[a,*], Bingsheng Huang, PhD[c,d,f,*], Shi-Ting Feng, MD, PhD[a,*]

Background: Tumor fibrosis plays an important role in chemotherapy resistance in pancreatic ductal adenocarcinoma (PDAC); however, there remains a contradiction in the prognostic value of fibrosis. The authors aimed to investigate the relationship between tumor fibrosis and survival in patients with PDAC, classify patients into high- and low-fibrosis groups, and develop and validate a CT-based radiomics model to non-invasively predict fibrosis before treatment.

Materials and methods: This retrospective, bicentric study included 295 patients with PDAC without any treatments before surgery. Tumor fibrosis was assessed using the collagen fraction (CF). Cox regression analysis was used to evaluate the associations of CF with overall survival (OS) and disease-free survival (DFS). Receiver operating characteristic (ROC) analyses were used to determine the rounded threshold of CF. An integrated model (IM) was developed by incorporating selected radiomic features and clinical-radiological characteristics. The predictive performance was validated in the test cohort (Center 2).

Results: The CFs were 38.22 ± 6.89% and 38.44 ± 8.66% in center 1 (131 patients, 83 males) and center 2 (164 patients, 100 males), respectively ($P = 0.814$). Multivariable Cox regression revealed that CF was an independent risk factor in the OS and DFS analyses at both centers. ROCs revealed that 40% was the rounded cut-off value of CF. IM predicted CF with areas under the curves (AUCs) of 0.829 (95% CI: 0.753-0.889) and 0.751 (95% CI: 0.677-0.815) in the training and test cohorts, respectively. Decision curve analyses revealed that IM outperformed radiomics model and clinical-radiological model for CF prediction in both cohorts.

Conclusions: Tumor fibrosis was an independent risk factor for survival of patients with PDAC, and a rounded cut-off value of 40% provided a good differentiation of patient prognosis. The model combining CT-based radiomics and clinical-radiological features can satisfactorily predict survival-grade fibrosis in patients with PDAC.

Keywords: fibrosis, pancreatic neoplasms, prognosis, radiomics

Introduction

Locally advanced disease or distant metastases are detected in ~80–85% of patients with pancreatic ductal adenocarcinoma (PDAC) at the time of the first visit; thus, radical resection is not a suitable treatment option for these patients[1]. Conventional cytotoxic chemotherapy is the standard treatment for patients with advanced or metastatic PDAC;

[a]Department of Radiology, The First Affiliated Hospital, Sun Yat-sen University, [b]State Key Laboratory of Oncology in South China, Collaborative Innovation Center for Cancer Medicine, Guangdong Key Laboratory of Nasopharyngeal Carcinoma Diagnosis and Therapy, Department of Radiology, Sun Yat-sen University Cancer Center, Guangzhou, [c]Marshall Laboratory of Biomedical Engineering, Shenzhen University, [d]Medical AI Lab, School of Biomedical Engineering, Shenzhen University Medical School, Shenzhen University, [e]South China Hospital, Medical School, Shenzhen University, [f]Shenzhen-Hong Kong Institute of Brain Science-Shenzhen Fundamental Research Institutions, [g]Shenzhen University Medical School, Shenzhen University and [h]National-Regional Key Technology Engineering Laboratory for Medical Ultrasound, Guangdong Key Laboratory for Biomedical Measurements and Ultrasound Imaging, Medical School, Shenzhen University, Shenzhen, Guangdong, China

S.S., R.L., J.Z. contributed equally to this article; thus, both should be considered as first authors.

Sponsorships or competing interests that may be relevant to content are disclosed at the end of this article.

*Corresponding author. Address: Department of Radiology, The First Affiliated Hospital, Sun Yat-sen University, No. 58, Second Zhongshan Road, Yuexiu District, Guangzhou, Guangdong, 510080, China. Tel.: +86 208 775 5766, extension 8471; fax: +86 208 761 5805. E-mail: fengsht@mail.sysu.edu.cn (S. T. Feng); Marshall Laboratory of Biomedical Engineering, Shenzhen University, 3688 Nanhai Avenue, Nanshan District, Shenzhen, Guangdong, 518055, China. Tel.: +86 075 586 172 208; fax: +86 861 716 20. E-mail: huangb@szu.edu.cn (B. Huang); Department of Radiology, The First Affiliated Hospital, Sun Yat-sen University, No. 58, Second Zhongshan Road, Yuexiu District, Guangzhou, Guangdong, 510080, China. Tel.: +86 208 775 5766, extension 8471; fax: +86 208 761 5805. E-mail: luoyj26@mail.sysu.edu.cn (Y. Luo).

International Journal of Surgery (2025) 111:950–961

Received 19 February 2024; Accepted 11 August 2024

Supplemental Digital Content is available for this article. Direct URL citations are provided in the HTML and PDF versions of this article on the journal's website, www.lww.com/international-journal-of-surgery.

Published online 22 August 2024

http://dx.doi.org/10.1097/JS9.0000000000002059

however, it only improves survival by a few months[2]. The desmoplastic reaction of the tumor results in an unsatisfactory treatment response[2], and pancreatic stellate cells activated by cancer cells induce fibrosis around the tumor cells[3]. The resultant desmoplasia creates a mechanical barrier around the tumor cells, which hinders vascularization, thereby leading to poor immune cell infiltration and limited drug delivery[4,5]. Nab-paclitaxel has distinct advantages in reducing cancer-associated fibroblasts and tumor fibrosis[6,7]. Compared with gemcitabine alone, nab-paclitaxel combined with gemcitabine (NG) chemotherapy regimens yield better survival in patients with metastatic PDAC[8]. NG regimens were reported to be more effective than other gemcitabine-based chemotherapy regimens in patients with locally advanced abundant stromal tumors in previous studies. However, this effect is not observed in tumors with poor stromal differentiation[9], emphasizing the importance of selecting appropriate treatments according to the grade of fibrosis surrounding the tumors. The dual effects of fibrosis on prognosis have been described in previous studies; however, the findings are inconsistent[2,10]. Some studies have reported that fibrosis is associated with poor prognosis[9,11,12], whereas other studies have reported that fibrosis has a tumor-promoting effect[13,14]. Thus, the role of fibrosis in prognosis must be investigated further.

Biopsies are performed to characterize and quantify fibrosis before surgery. However, this invasive procedure is not suitable for widespread use as it is prone to sampling bias, high risk, and high cost[15]. Previous studies have attempted to predict fibrosis preoperatively in patients with PDAC using non-invasive modalities, including clinical-radiological characteristics[16], computed tomography (CT) extracellular volume fraction[17], apparent diffusion coefficient value[18], dynamic contrast-enhanced and intravoxel incoherent motion MRI[19], and endoscopic ultrasonography elastography[9]. Nevertheless, these findings must be validated across different centers.

Radiomics extracts hundreds of quantitative features from medical images and combines key features with image-based biomarkers (radiomic features) for tumor characterization[20]. Radiomics has many applications in pancreatic diseases, such as predicting the occurrence of pancreatic cancer[21], evaluating the vascular invasion of pancreatic adenocarcinoma[22], and predicting the recurrence of PDAC after radical resection[23]. Previous studies have demonstrated the potential of radiomics as a tool for decoding the content of fibrosis in patients with PDAC before treatment.

It was hypothesized that tumor fibrosis could be classified into two survival-graded groups and that the incorporation of radiomics features and clinical-radiological features would help predict the status of fibrosis. Thus, the association between fibrosis and overall survival (OS)/disease-free survival (DFS) was determined, and the patients with PDAC were divided into high- and low-CF groups in this study. In addition, a CT-based radiomics model was developed and validated to non-invasively predict fibrosis before treatment in patients with PDAC from two centers. It was hypothesized that the performance of the integrated model would be superior to that of the clinical-radiological model.

HIGHLIGHTS

- To our best knowledge, this is the first bicentric study to investigate the relationship between tumor fibrosis and survival in patients with pancreatic ductal adenocarcinoma (PDAC), thus classifying patients into high- and low-fibrosis groups accordingly.
- The performance of our non-invasive model, incorporating the selected CT-based radiomic feature and clinical-radiological characteristics, could satisfactorily predict fibrosis before treatment and can be used as a supplement to treatment strategies decision and prognosis prediction in PDAC.

Material and methods

Patients

The Institutional Review Board of our hospital approved this retrospective study. The requirement for obtaining informed consent from the patients was waived. The study was conducted in line with the STROCSS criteria[23], Supplemental Digital Content 1, http://links.lww.com/JS9/D357. Patients with suspected pancreatic tumors who underwent contrast-enhanced CT and pathological examinations at Center 1 and Center 2 between January 2012 and January 2019 were eligible for inclusion in this study. The inclusion criteria were as follows: (a) pathologically diagnosed PDAC by resection; (b) patients were staged as resectable before surgery performed; (c) time intervals between contrast-enhanced CT and pathology less than 2 weeks; (d) no history of previous treatment such as resection, chemotherapy, or radiotherapy. The patients were excluded as follows: (a) unavailable pathological sections for evaluating the fibrosis; (b) incomplete clinical records; (c) missing CT images or poor CT image quality; (d) coincidence of other malignant tumors. In total, 131 and 164 patients were enrolled from Center 1 (training cohort) and Center 2 (test cohort), respectively. Figure 1 depicts a flowchart of the patient recruitment process.

Clinical-pathological variables were gathered, and radiological features were evaluated by three radiologists in consensus (Supplementary A1 and A2, Supplemental Digital Content 2, http://links.lww.com/JS9/D358, Supplementary Fig S1,

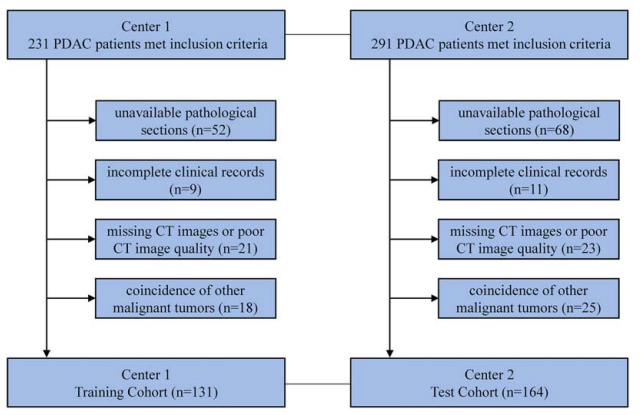

Figure 1. Flowchart of patient recruitment. CT, computed tomography; PDAC, pancreatic ductal adenocarcinoma.

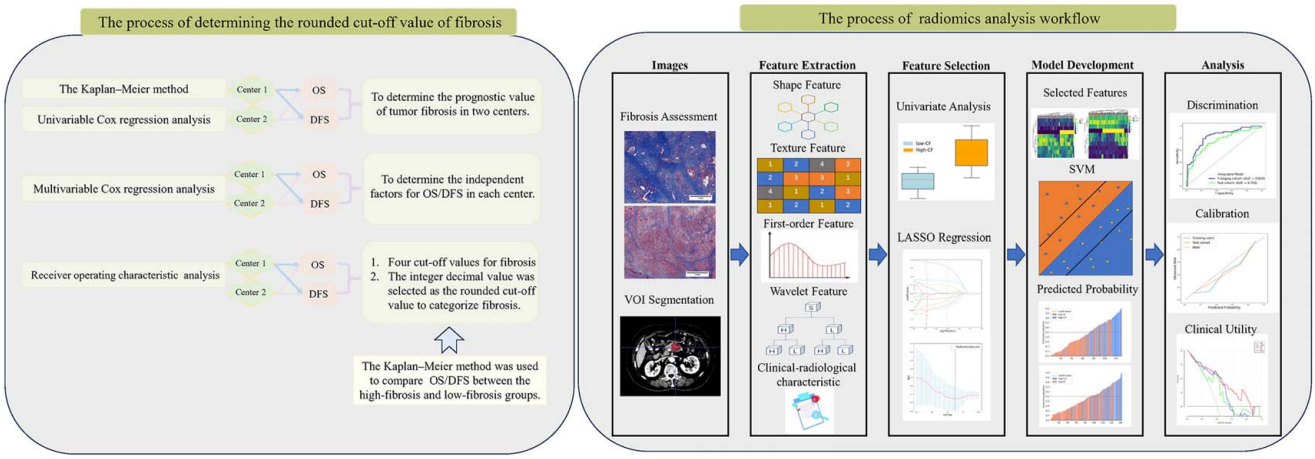

Figure 2. The process of statistical approach and radiomics analysis workflow. DFS, disease-free survival; OS, overall survival.

Supplemental Digital Content 2, http://links.lww.com/JS9/D358). The patients were followed up at 1, 3, 6, and 9 months postoperatively and every 3–6 months thereafter. All follow-up examinations included carbohydrate antigen 19-9 (CA 19-9) measurements and imaging (contrast-enhanced CT, contrast-enhanced MRI, ultrasonography, or positron emission tomography). The OS (death from time of pancreatic surgery) and DFS (recurrence or death from time of pancreatic surgery) were also recorded.

Fibrosis assessment

Tumor tissue specimens were fixed in 10% formalin and processed routinely. The tumor area with the richest fibrosis was selected[13], sectioned at a thickness of 4 μm, and stained using Masson's trichrome stain. The collagen fraction (CF), a quantitative substitute for fibrosis, was analyzed using ImageJ software (version 1.5; National Institutes of Health)[13]. Pathological images of 30 randomly selected patients were evaluated by two doctors blinded to the clinical-pathological data (Reader 1 and Reader 2 with 7 and 12 years of diagnostic pancreatic experiences, respectively). Reader 1 repeated the CF evaluation of the 30 patients two months later and completed the CF evaluation of the remaining patients. Interclass correlation coefficients (ICCs) were calculated to determine the inter-observer agreement for CF assessment.

CT parameters

Dual-phase enhanced CT examinations were performed using Aquilion One Vision (Canon Medical Systems), Aquilion Prime (Canon Medical Systems) at Center 1 and Brilliance iC (Philips Healthcare) and Discovery CT750 HD (GE Healthcare, USA) at Center 2. All patients were scanned in the supine position under breath-hold condition, covering the upper abdomen or entire abdomen. Venous images were used for radiomics analysis, as these images are commonly acquired for patients with PDAC across nearly all institutions[21]. Supplementary A3, Supplemental Digital Content 2, http://links.lww.com/JS9/D358 and Supplementary Table S1, Supplemental Digital Content 2, http://links.lww.com/JS9/D358 present the scanning protocols.

The association between fibrosis and survival

Univariable Cox regression analysis was used to evaluate the association of CF with OS/DFS. Multivariable Cox regression analysis was performed at each center using the forward likelihood-ratio method to identify the independent risk factors for OS/DFS. Receiver operating characteristic (ROC) analysis was used to evaluate the association between CF and the median OS/DFS. The values obtained for OS and DFS were analyzed and the threshold closest to the most frequently occurring round number was selected to determine the final threshold[24]. The Kaplan–Meier method was used to compare the difference in survival time between different CF grades in all patients and each center.

Development and validation of CT-based radiomics model

Volume-of-interest segmentation

The three-dimensional volume of interest (VOI) of the tumor was manually drawn on CT images by a radiologist (with 7 years of pancreatic diagnostic experience) using open-source software (ITK-SNAP, version 3.8.0; www.itksnap.org). The VOIs were drawn along the tumor contour in each transverse section until the entire tumor was captured. Thirty patients were randomly selected from the training cohort, and segmentation of the images of these patients was performed by the same radiologist and another radiologist (with 12 years of pancreatic diagnostic experience) to assess inter- and intra-observer reproducibility.

Radiomics feature extraction and selection

Radiomic features were extracted from the VOIs using an open-source pyradiomics toolkit (https://pyradiomics.readthedocs.io/en/v1.0/installation.html). In total, 1130 quantitative radiomics features, including shape, texture, first-order, and wavelet features, were extracted for each VOI. The min-max scaling method was used to normalize the radiomic features.

The following feature selection strategies were used to reduce the dimensionality and select the best subset of radiomics features: selecting features under a significance level of 0.05 between low-CF and high-CF in the training cohort according to the

Table 1

The clinicopathological data in two centers.

Variables	Total ($n=295$)	Center 1 ($n=131$)	Center 2 ($n=164$)	P
Sex, *n* (%)				0.765
Female	112 (38)	48 (37)	64 (39)	
Male	183 (62)	83 (63)	100 (61)	
Age, mean ± SD	59.52 ± 10.57	60.34 ± 10.54	58.86 ± 10.58	0.232
BMI, mean ± SD	22.37 ± 2.83	22.57 ± 2.84	22.21 ± 2.82	0.278
Diabetes, *n* (%)				0.393
No	233 (79)	100 (76)	133 (81)	
Yes	62 (21)	31 (24)	31 (19)	
Smoking, *n* (%)				0.450
No	220 (75)	101 (77)	119 (73)	
Yes	75 (25)	30 (23)	45 (27)	
Jaundice, *n* (%)				0.446
No	130 (44)	54 (41)	76 (46)	
Yes	165 (56)	77 (59)	88 (54)	
Ache, *n* (%)				0.390
No	149 (51)	62 (47)	87 (53)	
Yes	146 (49)	69 (53)	77 (47)	
CA 19-9, *n* (%)				0.554
No	64 (22)	31 (24)	33 (20)	
Yes	231 (78)	100 (76)	131 (80)	
PTCD, *n* (%)				0.840
No	248 (84)	109 (83)	139 (85)	
Yes	47 (16)	22 (17)	25 (15)	
Surgical approach, *n* (%)				0.011*
No	69 (23)	21 (16)	48 (29)	
Yes	226 (77)	110 (84)	116 (71)	
Blood transfusion, *n* (%)				0.108
No	203 (69)	97 (74)	106 (65)	
Yes	92 (31)	34 (26)	58 (35)	
POPF				0.926
No	245 (83)	108 (82)	137 (84)	
Yes	50 (17)	23 (18)	27 (16)	
Postoperative chemotherapy, *n* (%)				0.033*
No	170 (58)	85 (65)	85 (52)	
Yes	125 (42)	46 (35)	79 (48)	
Resection margin, *n* (%)				> 0.999
R0	273 (93)	121 (92)	152 (93)	
R1	22 (7)	10 (8)	12 (7)	
Location, *n* (%)				0.011*
Body/tail	59 (20)	17 (13)	42 (26)	
Head/uncinate	236 (80)	114 (87)	122 (74)	
Differentiation, *n* (%)				0.061
Well	10 (3)	4 (3)	5 (3)	
Moderate	154 (52)	77 (59)	75 (46)	
Poor	131 (44)	50 (38)	84 (51)	
pT, *n* (%)				0.017*
1	8 (3)	3 (2)	5 (3)	
2	84 (28)	33 (25)	51 (31)	
3	184 (62)	92 (70)	92 (56)	
4	19 (6)	3 (2)	16 (10)	
pN, *n* (%)				< 0.001*
0	162 (55)	87 (66)	75 (46)	
Other	133 (45)	44 (34)	89 (54)	
CF, Mean ± SD *n* (%)	38.35 ± 7.91	38.22 ± 6.89	38.44 ± 8.66	0.814
Perineural invasion, *n* (%)				< 0.001*
No	104 (35)	71 (54)	33 (20)	
Yes	191 (65)	60 (46)	131 (80)	

Table 1

(*Continued*)

*$P < 0.05$.

Continuous variables are described as mean ± standard deviation (normally distributed) and median (interquartile range) (not normally distributed) and compared using an unpaired, two-tailed *t*-test or a Mann–Whitney U test.

Categorical variables are presented as numbers (percentage) and compared using the χ^2 test or Fisher's exact test.

CA, carbohydrate antigen; CF, collagen fraction; pN, pathological N stage; POPF, postoperative pancreatic fistula; pT, pathological T stage; PTCD, percutaneous transhepatic cholangial drainage.

Surgical approaches were grouped as pancreaticoduodenectomy and non-pancreaticoduodenectomy.

Mann–Whitney U test or Student's *t*-test; the least absolute shrinkage and selection operator (Lasso) of the logistic regression model was applied to select CF-related features.

Clinical-radiological characteristic selection

Three continuous clinical characteristics were normalized using the min-max scaling method. Clinical-radiological characteristics were selected using the Mann–Whitney U test, Student's *t*-test, or χ^2 test according to the data distribution in the training cohort to construct the clinical-radiological model (CRM).

Development and validation of radiomics models

A binary classification radiomics model (RM) was built using a support vector machine (SVM) to distinguish between low and high CF based on the radiomic features selected. Leave-one-out cross-validation was performed in the training cohort to avoid overfitting and select the best parameters for RM. The optimal parameters, comprising C (regularization parameter), gamma (kernel coefficient), tol (tolerance for stopping criteria), class-weight (weight of class), and max_iter (hard limit on iterations within the solver) in the SVM model, were identified using the grid search method. The overall prediction performance in the training cohort was assessed based on the probabilities of the test samples in each fold during cross-validation. The prediction probability for each case in the test cohort was determined by averaging the prediction probabilities from all models during training. An integrated model (IM) was developed using the same approaches and incorporating both radiomics features and clinical-radiological characteristics. The models (CRM, RM, and IM) were validated using a completely independent test cohort. The Kaplan–Meier method was used to compare the differences in survival time between the different CF-predicted grades in all patients.

Model development was performed in Python (version 3.9; https://www.python.org/) using the Scikit-learn package (version 1.1.2; https://www.scikit-learn.org/). Figure 2 presents the workflow of the radiomics analysis.

Statistical analysis

Supplementary A4, Supplemental Digital Content 2, http://links.lww.com/JS9/D358 presents the sample size evaluation. The

Table 2

Univariable and multivariable cox regression for clinical-pathological variables and survival in two centers.

Survival	Variable	HR (univariable)	HR (multivariable)
Center 1 OS	CF	1.12 (1.08–1.16, $P<0.001^*$)	1.14 (1.10–1.18, $P<0.001^*$)
	Ache	1.80 (1.20–2.71, $P=0.005^*$)	1.85 (1.19–2.86, $P=0.006^*$)
	Blood transfusion	1.57 (1.01–2.45, $P=0.047^*$)	1.35 (0.83–2.20, $P=0.230$)
	Differentiation	1.52 (1.04–2.20, $P=0.029^*$)	1.69 (1.13–2.51, $P=0.010^*$)
	pT	1.54 (1.03–2.31, $P=0.035^*$)	1.37 (0.88–2.11, $P=0.160$)
Center 1 DFS	CF	1.11 (1.07–1.15, $P<0.001^*$)	1.12 (1.07–1.17, $P<0.001^*$)
	Ache	1.81 (1.11–2.95, $P=0.017^*$)	1.48 (0.91–2.41, $P=0.116$)
	pN	1.74 (1.06–2.83, $P=0.027^*$)	2.07 (1.25–3.44, $P=0.005^*$)
Center 2 OS	CF	1.13 (1.10–1.16, $P<0.001^*$)	1.13 (1.10–1.16, $P<0.001^*$)
	Postoperative chemotherapy	0.64 (0.41–0.99, $P=0.047^*$)	0.36 (0.22–0.58, $P<0.001^*$)
Center 2 DFS	CF	1.12 (1.09–1.15, $P<0.001^*$)	1.12 (1.09–1.15, $P<0.001^*$)
	Differentiation	1.56 (1.06–2.29, $P=0.023^*$)	1.36 (0.91–2.04, $P=0.133$)
	pN	1.55 (1.01–2.37, $P=0.044^*$)	1.54 (1.00–2.36, $P=0.051$)

$^*P<0.05$.

CF, collagen fraction; DFS, disease-free survival; HR, hazard ratio; OS, overall survival; pN, pathological N stage; pT, pathological T stage.

discrimination performance of the models was evaluated using the area under the receiver operating characteristic (ROC) curve (AUC), reported with corresponding 95% CIs. The accuracy, sensitivity, and specificity were calculated from the ROC curve based on the cut-off value that maximized the Youden index. Paired and unpaired ROC curves were compared between the different models using DeLong's method. The Hosmer-Lemeshow goodness-of-fit test was used to assess the calibration performance of the IM. Decision curve analysis was used to evaluate the clinical utility of the three models (Supplementary A5, Supplemental Digital Content 2, http://links.lww.com/JS9/D358). A two-sided P value less than 0.05 was considered statistically significant. All statistical analyses were performed using R (version 4.1.2; http://www.r-project.org/), SPSS (version 24.0; https://www.ibm.com/analytics/spss-statistics-software/), and MedCalc (version 15.8; http://www.medcalc.org/).

Results

Determination of CF grading threshold

Eighty-three males and 48 females from center 1 (age, 60.34 ± 10.54 years old), and 100 males and 64 females from center 2 (age, 58.86 ± 10.58 years old) were included in this study (Table 1). The 3-year and 5-year survival rates were 18.32% and 8.88%, respectively, in center 1 and 31.2% and 21.4% in center 2, respectively. No statistical differences were observed between centers 1 and 2 in terms of OS (median months, 16.23 vs. 20.13, $P=0.050/0.232$ in the Log Rank test/Breslow test) or DFS (median months, 9.87 vs. 10.73, $P=0.731/0.619$ in the Log Rank test/Breslow test). The hazard ratios of fibrosis for OS and DFS were 1.12 (95% CI: 1.08–1.16) and 1.11 (95% CI: 1.07–1.15) in the training cohort and 1.13 (95% CI: 1.10–1.16) and 1.12 (95% CI: 1.09–1.15) in the test cohort, respectively, indicating its association with a poor prognosis.

Table 3

ROC analysis of the collagen fraction for median overall survival and disease-free survival.

		ROC analysis			
Hospital	Survival	Cut-off point	AUC (95% CI)	Se	Sp
Center 1	OS	41.44%	0.666 (0.574–0.757)	0.462	0.803
	DFS	39.88%	0.707 (0.618–0.797)	0.646	0.788
Center 2	OS	34.94%	0.834 (0.766–0.903)	0.767	0.818
	DFS	36.59%	0.840 (0.779–0.901)	0.722	0.878

AUC, area under the curve; DFS, disease-free survival; OS, overall survival; ROC, operator characteristic curve; Se, sensitivity; Sp, specificity.

The ICC for CF assessment was 0.897 ($P < 0.001$). The CFs were 38.22 ± 6.89% and 38.44 ± 8.66% in center 1 and center 2, respectively ($P=0.814$). Multivariable Cox regression analysis performed after univariable analysis (Supplementary Table S2, Supplemental Digital Content 2, http://links.lww.com/JS9/D358) revealed that CF was an independent prognostic factor for OS and DFS analyses at both centers (Table 2). The cut-off values of ROCs for CF and OS/DFS were 41.44%/39.88% and 34.94%/36.59% in centers 1 and 2, respectively (Table 3 and Fig. 3). The integer decimal value 40% was selected as the rounded cut-off value for CF for ease of use, and the patients were divided into high-CF and low-CF groups[24]. The Kaplan–Meier method revealed statistically significant differences in OS/DFS between the high-CF and low-CF groups (Supplementary Table S3, Supplemental Digital Content 2, http://links.lww.com/JS9/D358 and Fig. 3). Table 4 presents the clinical-pathological and radiological features.

Development and validation of RM and CRM

Radiomics feature selection

Among the 1130 radiomics features extracted from the training cohort, 18 features with a significance level of 0.05 between low-CF and high-CF groups were included in the following analysis. The LASSO model was built subsequently, and eight CF-related features were selected from the training cohort (Supplementary Fig S2A and 2B, Supplemental Digital Content 2, http://links.lww.com/JS9/D358). Supplementary Table S4, Supplemental Digital Content 2, http://links.lww.com/JS9/D358 presents the selected radiomic features. Supplementary Fig S2C and 2D, Supplemental Digital Content 2, http://links.lww.com/JS9/D358 present the heatmaps of the selected features in both cohorts.

Clinical-radiological characteristic selection

Among the 16 clinical-radiological characteristics, tumor diameter and peripancreatic tumor infiltration were selected for the

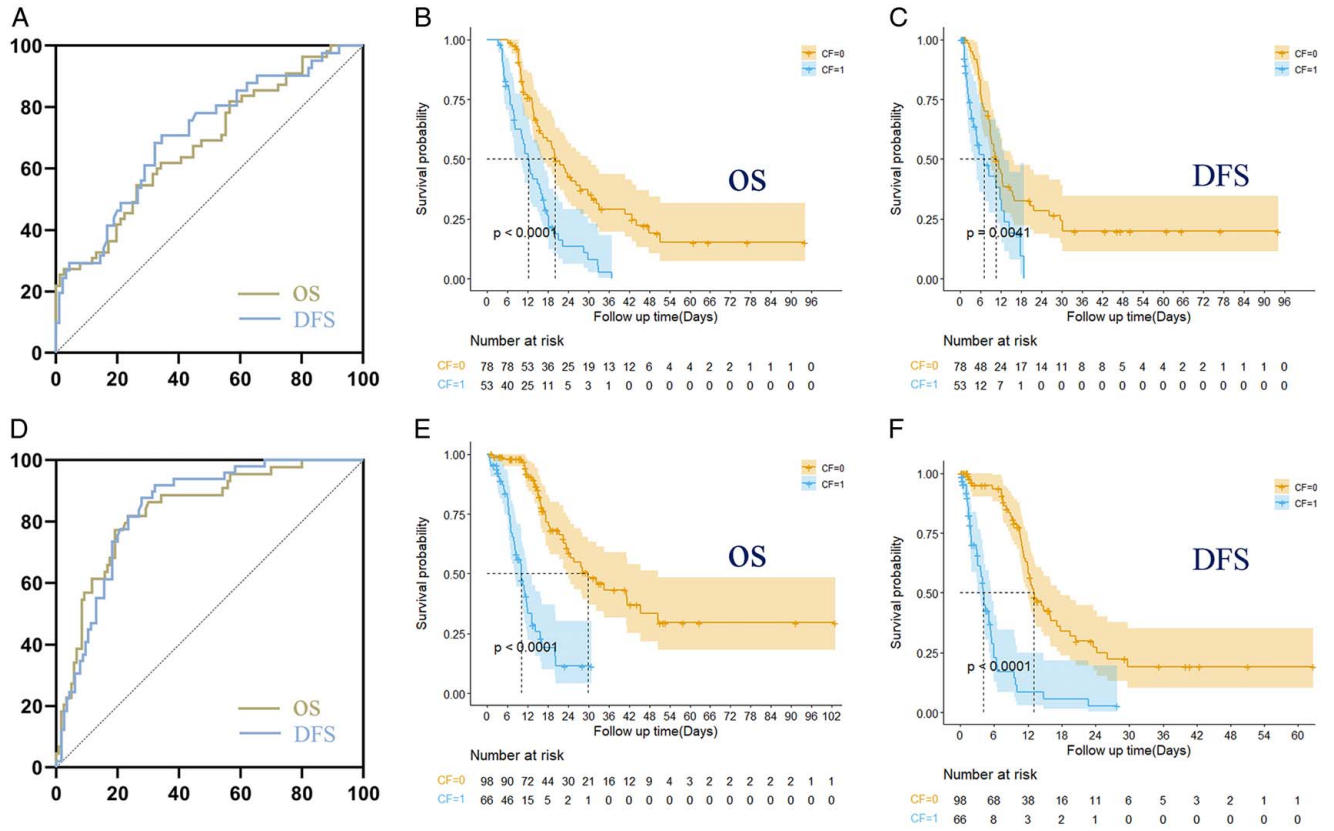

Figure 3. Univariable cox regression analysis of collagen fraction and overall survival/disease-free survival in both cohorts. (A, D) The receiver operating characteristic curve of collagen fraction for predicting overall survival/disease-free survival in the training and test cohorts. (B, C) The Kaplan–Meier survival analysis of overall survival/disease-free survival between different collagen fraction groups using a threshold of 40% in the training cohort. (E, F) The Kaplan–Meier survival analysis of overall survival/disease-free survival between different collagen fraction groups using a threshold of 40% in the test cohort. DFS, disease-free survival; OS, overall survival.

development of CRM and IM based on the results of univariable analysis. Table 4 presents the selected characteristics. Supplementary Fig S2C and 2D, Supplemental Digital Content 2, http://links.lww.com/JS9/D358 present the heatmaps of the selected characteristics in both cohorts.

Development of RM and CRM

The SVM model was trained to achieve the best performance based on the training cohort and then applied to an independent test cohort. The output of the model was generated as a non-linear combination of CF-related features with a value between zero and one, denoting the predicted probability of survival-graded fibrosis. The best cut-off values for dividing the patients into low-CF and high-CF groups in RM and CRM were 0.411 and 0.480, respectively.

Predictive performance in validation of RM and CRM

RM and CRM predicted survival-graded fibrosis with AUCs of 0.760 (95% CI, 0.678–0.830, $P < 0.001$) and 0.765 (95% CI, 0.683–0.834, $P < 0.001$) in the training cohort and AUCs of 0.656 (95% CI, 0.578–0.729, $P < 0.001$) and 0.708 (95% CI, 0.632–0.776, $P < 0.001$) in the independent test cohort, respectively (Table 5 and Figs. 4A and B).

Development and validation of IM

Development of IM

Eight radiomic features, with an additional two clinical-radiological characteristics, were used to build the IM using the same modeling process that was used to build RM and CRM, and the best cut-off value for the IM was 0.500.

Predictive performance in validation of IM

IM predicted survival-graded fibrosis with an AUC of 0.829 (95% CI, 0.753–0.889, $P < 0.001$) and 0.751 (95% CI: 0.677–0.815, $P < 0.001$) in the training and test cohorts, respectively (Fig. 4C, Table 5). DeLong's test revealed no significant difference between the ROC curves of the training and test cohorts ($P = 0.198$), suggesting considerable efficacy and robustness of IM (Fig. 4C). The Hosmer-Lemeshow test yielded a χ^2 value of 5.239 ($P = 0.155$) and 4.496 ($P = 0.213$) in the training cohort and test cohort, suggesting good fit (Fig. 4J). Figure 5 presents two representative cases of IM classification.

Statistically significant differences were observed between IM-negative prediction and IM-positive prediction in the total cohort on comparing OS (median months, 28.83 vs. 13.43, both $P < 0.001$ of Log Rank test and Breslow test) or DFS (median

Table 4

Univariable logistic analysis of collagen fraction and clinical-radiological features in both centers.

	Training cohort			Test cohort		
Variables	**Low-CF (*n* = 78)**	**High-CF (*n* = 53)**	***P*[a]**	**Low-CF (*n* = 98)**	**High-CF (*n* = 66)**	***P*[a]**
Sex, *n* (%)			0.187			0.062
Female	25 (32)	23 (43)		44 (45)	20 (30)	
Male	53 (68)	30 (57)		54 (55)	46 (70)	
Age, mean ± SD	60.42 ± 10.56	60.23 ± 10.62	0.916	58.23 ± 11.11	59.79 ± 9.74	0.356
BMI, mean ± SD	22.7 ± 2.78	22.39 ± 2.94	0.543	22.29 ± 2.82	22.1 ± 2.83	0.664
Diabetes, *n* (%)			0.848			0.155
No	60 (77)	40 (75)		83 (85)	50 (76)	
Yes	18 (23)	13 (25)		15 (15)	16 (24)	
Smoking, *n* (%)			0.954			0.500
No	60 (77)	41 (77)		73 (74)	46 (70)	
Yes	18 (23)	12 (23)		25 (26)	20 (30)	
Jaundice, *n* (%)			0.677			0.276
No	31 (40)	23 (43)		42 (43)	34 (52)	
Yes	47 (60)	30 (57)		56 (57)	32 (48)	
Ache, *n* (%)			0.699			0.111
No	38 (49)	24 (45)		57 (58)	30 (45)	
Yes	40 (51)	29 (55)		41 (42)	36 (55)	
CA 19-9, *n* (%)			0.061			0.911
No	23 (29)	8 (15)		20 (20)	13 (20)	
Yes	55 (71)	45 (85)		78 (80)	53 (80)	
PTCD, *n* (%)			0.320			0.979
No	67 (86)	42 (79)		83 (85)	56 (85)	
Yes	11 (14)	11 (21)		15 (15)	10 (15)	
Location, *n* (%)			0.948			0.260
Body/tail	10 (13)	7 (13)		22 (22)	20 (30)	
Head/uncinate	68 (87)	46 (87)		76 (78)	46 (70)	
Diameter, median (Q1, Q3)	24.5 (19, 28)	32 (25, 40)	< 0.001	31 (24.25, 39)	32.5 (26, 40.75)	0.709
Necrosis, *n* (%)			0.158			0.655
No	48 (62)	26 (49)		47 (48)	34 (52)	
Yes	30 (38)	27 (51)		51 (52)	32 (48)	
PTI, *n* (%)			< 0.001			< 0.001
No	57 (73)	22 (42)		61 (62)	13 (20)	
Yes	21 (27)	31 (58)		37 (38)	53 (80)	
cN, *n* (%)			0.322			0.048
No	48 (62)	28 (53)		23 (23)	25 (38)	
Yes	30 (38)	25 (47)		75 (77)	41 (62)	
MPD, *n* (%)			0.653			0.775
No	11 (14)	9 (17)		19 (19)	14 (21)	
Yes	67 (86)	44 (83)		79 (81)	52 (79)	
Bile duct dilation, *n* (%)			0.255			0.073
No	29 (37)	25 (47)		38 (39)	35 (53)	
Yes	49 (63)	28 (53)		60 (61)	31 (47)	
Atrophy, *n* (%)			0.231			0.689
No	48 (62)	38 (72)		74 (76)	48 (73)	
Yes	30 (38)	15 (28)		24 (24)	18 (27)	

CA, carbohydrate antigen; CF, collagen fraction; cN, CT-based suspicious metastatic lymph nodes; MPD, main pancreatic dilation; OR, odds ratio; PTCD, percutaneous transhepatic cholangial drainage; PTI, peripancreatic tumor infiltration.

[a]*P* value was calculated using univariable logistic analyses between each characteristic and CF status.

months, 11.50 vs. 7.10, $P = 0.001/< 0.001$ in the Log Rank test/ Breslow test).

Comparison of IM, RM, and CRM

Diagnostic performance comparison

IM vs. RM. Compared with RM, IM demonstrated superior predictive performance for survival-graded fibrosis in the training cohort (AUC = 0.829 vs. AUC = 0.760, $P = 0.329$; Fig. 4D) and test cohort (AUC = 0.751 vs. AUC = 0.656, $P = 0.065$; Fig. 4E); however, the differences were not statistically significant.

IM vs. CRM. Compared with CRM, IM exhibited superior performance in the training cohort (AUC = 0.829 vs. AUC = 0.765, $P = 0.136$; Fig. 4D) and test cohort (AUC = 0.751 vs. AUC = 0.708, $P = 0.214$; Fig. 4E); however, the differences were not statistically significant.

Figure 6 presents the contributions of the different modalities and the top five important features of the three models.

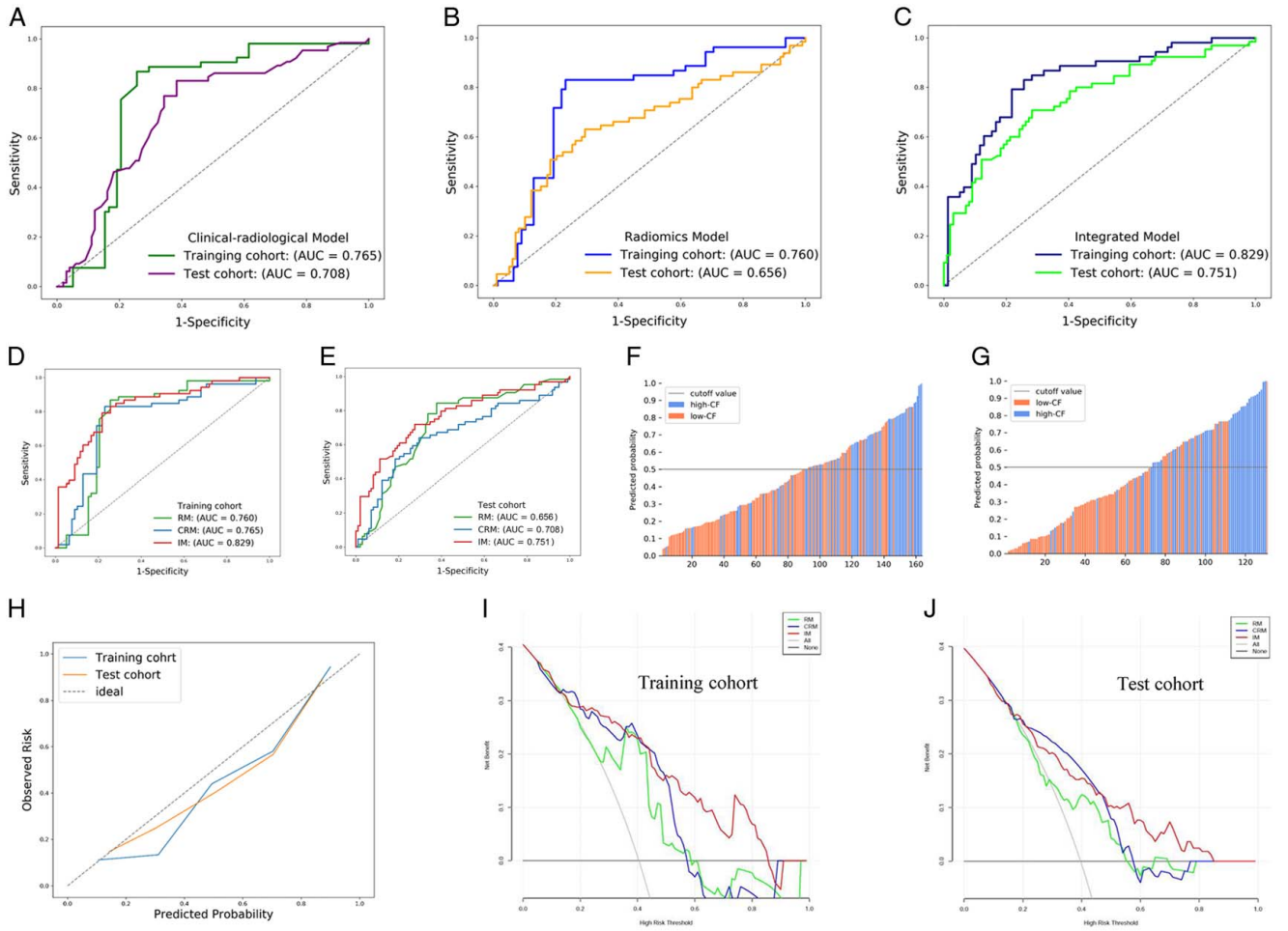

Figure 4. Predictive performance of the clinical-radiological, radiomics, and integrated models in the training and test cohorts. (A) The receiver operating characteristic (ROC) curves of the clinical-radiological model in both cohorts. (B) The ROCs of the radiomics model in both cohorts. (C) The ROCs of the integrated model in both cohorts. (D) The ROCs of different models in the training cohort. (E) The ROCs of different models in the test cohort. (F, G) The predicted probability in the training cohort and test cohorts. Orange color represents the true low collagen fraction group, whereas blue color represents the high collagen fraction group. (H) The calibration curves in the training and test cohorts. (I, J) The decision curve analysis in the training and test cohorts. AUC, area under the curve; CF, collagen fraction.

Clinical utility comparison

IM consistently provided a better net benefit in predicting survival-graded fibrosis than RM in the training and test cohorts according to the decision curve analysis (Figs. 4H and I). Furthermore, decision curve analysis revealed that the IM group had a better net benefit than the CRM group in the training

Table 5

Prediction performance of the models.

Variable	AUC (95%CI)	Accuracy	Sensitivity	Specificity	*P*[a]
Training cohort ($n = 131$)					
Radiomics model	0.760 (0.678–0.830)	0.794	0.830	0.769	< 0.001
Clinical-radiological model	0.765 (0.683–0.834)	0.794	0.868	0.744	< 0.001
Integrated model	0.829 (0.753–0.889)	0.786	0.792	0.782	< 0.001
Test cohort ($n = 164$)					
Radiomics model	0.656 (0.578–0.729)	0.659	0.631	0.677	< 0.001
Clinical-radiological model	0.708 (0.632–0.776)	0.695	0.831	0.606	< 0.001
Integrated model	0.751 (0.677–0.815)	0.713	0.708	0.717	< 0.001

The accuracy, sensitivity, and specificity of the radiomics, clinical-radiological, and integrated models were 0.411, 0.480, and 0.500, respectively, which maximized the Youden index in the training cohort. AUC, area under the curve.

[a]*P* value is the significance level of comparison of the AUC with that of the random case (AUC = 0.5).

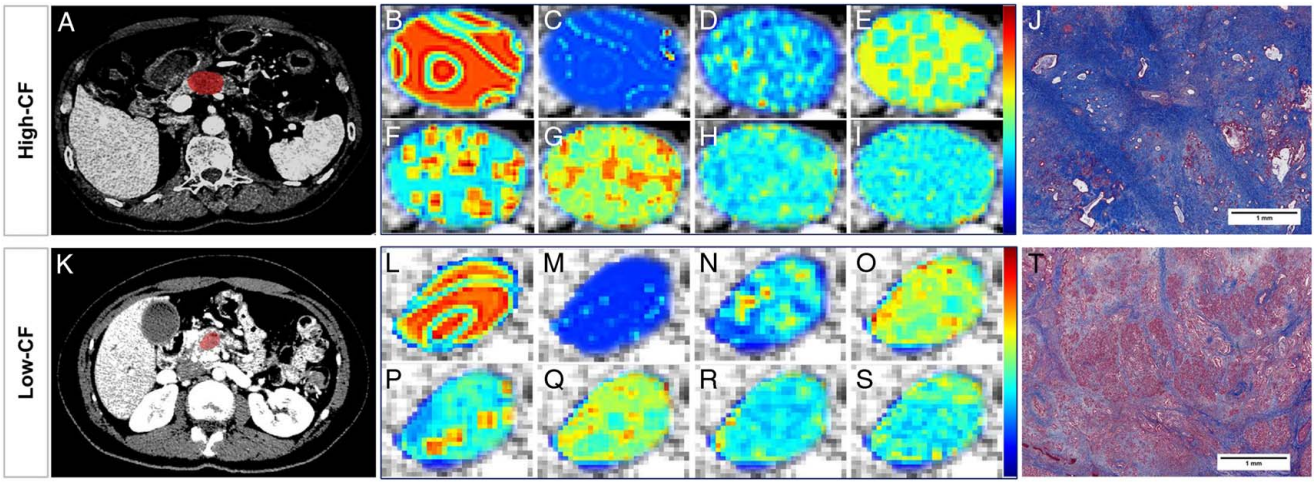

Figure 5. Representative patients with high collagen fraction (CF). [(A–J); predicted probability of CF = 0·800) and with low-CF [(K–T); predicted probability of CF = 0·210).

Model	Modalities	Features	Top 5 important features	Contribution of different modalities
RM	Radiomics Features	8	(1) wavelet-LLL_glszm_SizeZoneNonUniformityNormalized (2) log-sigma-5-0-mm-3D_glszm_SmallAreaLowGrayLevelEmphasis (3) wavelet-HLH_glszm_LowGrayLevelZoneEmphasis (4) wavelet-HLH_gldm_DependenceVariance (5) wavelet-HLH_glszm_GrayLevelNonUniformityNormalized	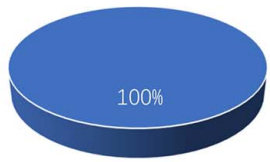
CRM	Clinical-radiological Characteristics	2	(1) PTI (2) diameter	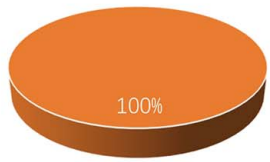
IM	Radiomics Features Clinical-radiological Characteristics	10	(1) wavelet-LLL_glszm_SizeZoneNonUniformityNormalized (2) log-sigma-5-0-mm-3D_glszm_SmallAreaLowGrayLevelEmphasis (3) wavelet-HLH_glszm_LowGrayLevelZoneEmphasis (4) wavelet-HLH_gldm_DependenceVariance (5) wavelet-HLH_glszm_GrayLevelNonUniformityNormalized	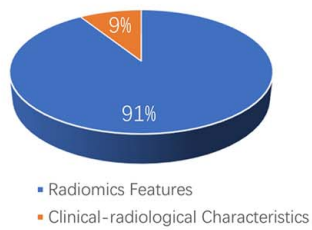

Figure 6. Contribution of different modalities and the five most important features in the three models. CRM, clinical-radiological model; IM, integrated model; PTI, peripancreatic infiltration; RM, radiomics model.

group. IM outperformed CRM in the test cohort in terms of net benefit when the threshold probability exceeded ~45%.

Discussion

The findings of the present study suggest that tumor fibrosis is a prognostic risk factor for PDAC and can be used to classify patients into high- and low-fibrosis groups. An integrated model based on CT data that combined radiomics and clinical-radiological features was developed and validated to predict survival-graded fibrosis. This model demonstrated a high performance in predicting survival-graded fibrosis across the two institutions. Decision curve analysis revealed that the integrated model outperformed the radiomics and clinical-radiological models in terms of the net benefit for fibrosis prediction in the training and test cohorts.

Patients with significant fibrosis had poor prognosis in this bicentric study, which was consistent with the results of previous studies[9,12,14,24]. The multivariable cox analysis results indicated that ache[25], differentiation[26], pathological N stage[27], postoperative chemotherapy[28] were independent factors of

survivals, in addition to fibrosis, as previous studies shown. Previous studies[29,30] also suggested that postoperative pancreatic fistula (POPF) was risk prognostic factor but not in our studies. It might be due to very low occurrence rate (3.7%, 11/295) of patients with grade C of POPF in our study. Patients with grade B of POPF were managed in a timely management after surgery. Consequently, the OS and DFS of patients with POPF at these two centers did not show significantly shortening. However, tumor fibrosis was the only prognostic factor present in the multivariable cox analysis for both centers, indicating that tumor fibrosis affects prognosis independently of other clinical-pathological factors, thereby confirming the tumor-promoting nature of fibrosis. Moreover, the tumor fibrosis quantified in this study could be classified as high- or low-grade based on its association with survival, providing a referable way to determine a threshold of 40%, consistent with the findings of a previous baseline, single-center study[16]. Another study reported a grading threshold of 70% for tumor fibrosis according to survival in patients after chemoradiotherapy[13], which was attributed to the increased fibrosis of tumors after chemoradiotherapy.

The findings of the present study revealed that the tumor diameter and peripancreatic tumor infiltration, which reflect tumor malignancy, were correlated with fibrosis. A dense fibrotic microenvironment can disrupt oxygen supply by applying mechanical stress to the tumor vasculature, which reduces tissue perfusion and induces hypoxia[31]. Hypoxia promotes PDAC progression by facilitating its invasiveness and metastasis[32,33]. The presence and spatial organization of collagen play an important role in the development of cancer. Collagen fibers in PDAC present a characteristic topology, especially around the malignant ducts, characterized by a high degree of alignment and increased length and width[34]. This unique organization of collagen promotes tumor growth and aggressive formation, often resulting in poor prognosis[35]. Furthermore, a significant interaction was observed between fibroblasts and tumor cells. Pancreatic stellate cells are myofibroblast-like cells that were initially considered the source of fibrosis in patients with chronic pancreatitis. However, they are responsible for the formation of dense mesenchymal stroma associated with PDAC now. Co-injection of PDAC tumor cells and human pancreatic stellate cells, the primary source of type I collagen, into an in-situ mouse model resulted in increased tumor incidence, size, and metastasis[4]. Thus, the characteristics reflecting tumor aggressiveness correlate with tumor fibrosis and can be used to assess tumor fibrosis.

Dense fibrosis is the most characteristic pathologic feature of PDAC. Dense fibrosis may trap proangiogenic molecules in the matrix, thereby limiting their ability to trigger angiogenesis[36,37]. Fibrosis-induced low vessel density affects tumor enhancement, and most radiomic features are highly sensitive to changes in image intensity[38,39]. In addition, the predominance of fibrosis in PDAC leads to significant tumor spatial heterogeneity[36], and texture features are widely used as predictors of tumor heterogeneity[40]. The leave-one-out cross-validation method used in this study is more suitable for small datasets as more data can be used for training, thereby improving estimated classification accuracy[41,42]. Furthermore, voxel-wise tumor heterogeneity mapping enables direct visualization and interpretation of features that can be used more reliably in clinical practice[43]. Meng *et al.*[12,24]. reported that CT- or MR-based radiomics could be used to predict the tumor-stroma ratio in patients with PDAC, confirming the potential of radiomic features as a tool for decoding the PDAC tumor microenvironment. However, the tumor-to-stroma ratio is affected by several components, including immune cells, which have a more complex prognostic impact, and the two studies were single-center studies without independent validation sets.

The non-invasive, accurate integrated model developed in this study paves the way for tumor fibrosis prediction. To the best of our knowledge, this study is the first to construct a CT-based radiomics model to predict survival-graded fibrosis before treatment in patients with PDAC from two centers. Second, the survival-graded fibrosis predicted using the proposed model achieved satisfactory predictive performance in the training group and good predictive efficacy in the validation group at another center. In addition, this model has the potential to be widely used in clinical practice owing to the large sample size. Furthermore, tumor size and peripancreatic tumor infiltration were included as radiomics features in the integrated model to predict fibrosis. This considered real-world situations and was more relevant to the practical work of radiologists. Lastly, IM could discriminate OS and DFS in the total cohort, suggesting that it is predictive of prognosis.

This study had some limitations. First, the retrospective study design may have introduced patient selection bias. Second, only a few patients with well-differentiated PDAC were selected from the two centers in this study. Future studies should include more patients with well-differentiated PDAC. Lastly, the segmentation of the tumor on CT images and pathological fibrosis sampling did not correspond, owing to the enormous pathological workload.

In conclusion, tumor fibrosis was categorized into high and low grade according to its relationship with survival in patients with PDAC, and an integrated model, comprising CT-based radiomics and clinical-radiological features was developed to predict tumor fibrosis in this study. This model can serve as an auxiliary tool for the formulation of personalized chemotherapy strategies and prognosis prediction in patients with PDAC.

Ethical approval

This retrospective study was approved by the Institutional Review Board of the First Affiliated Hospital, Sun Yat-sen University, Guangdong, China on 13 January 2021 (approval number: 2021 [025]).

Consent

The requirement for obtaining informed consent from the patients was waived due to the retrospective design.

Source of funding

This work was supported in part by the National Natural Science foundation of China (Grant Number 81801761 to Y.L., 62371303 to B.H., and Grant Number 82271958 to S.-T.F.), Marshall Lab of Biomedical Engineering open fund: Medical-Engineering Project (to B.H.), and the Shenzhen-Hong Kong Institute of Brain Science-Shenzhen Fundamental Research Institutions of China (Grant Number 2023SHIBS0003 to J.Z.).

Author contribution

Conception and design of the study: S.S., R.L., J.Z., Y.L., B.H., S.-T.F. Data collection: S.S., Y.L., J.Z., S.-T.F., J.L. Data analyses: R. L., H.L., J.M., J.Z., X.D., B.H. Manuscript preparation: S.S., R.L., J.Z., J.L., Y.L., B.H., S.-T.F. Supervision and project administration: S.-T.F., B.H., Y.L.

Conflicts of interest disclosure

The authors declare no conflicts interest.

Research registration unique identifying number (UIN):

- Name of the registry: A CT-based Radiomics Model to Predict Survival-graded Fibrosis in PDAC.
- Unique identifying number or registration ID: NCT062 67690.
- Hyperlink to your specific registration (must be publicly accessible and will be checked) : ClinicalTrials.gov PRS: Record Summary NCT06267690.

Guarantor

All the authors took responsibility of the final manuscript and approved it for publication.

Data availability statement

All data generated for this study are included in the article or Supplementary Material and from the corresponding author upon reasonable request.

Provenance and peer review

Our paper was not invited.

References

[1] Park W, Chawla A, O'Reilly EM. Pancreatic cancer: a review. JAMA 2021;326:851–62.

[2] Ho WJ, Jaffee EM, Zheng L. The tumour microenvironment in pancreatic cancer—clinical challenges and opportunities. Nat Rev Clin Oncol 2020; 17:527–40.

[3] Vonlaufen A, Joshi S, Qu C, *et al*. Pancreatic stellate cells: partners in crime with pancreatic cancer cells. Cancer Res 2008;68:2085–93.

[4] Hwang RF, Moore T, Arumugam T, *et al*. Cancer-associated stromal fibroblasts promote pancreatic tumor progression. Cancer Res 2008;68: 918–26.

[5] Provenzano PP, Cuevas C, Chang AE, *et al*. Enzymatic targeting of the stroma ablates physical barriers to treatment of pancreatic ductal adenocarcinoma. Cancer Cell 2012;21:418–29.

[6] Alvarez R, Musteanu M, Garcia-Garcia E, *et al*. Stromal disrupting effects of nab-paclitaxel in pancreatic cancer. Br J Cancer 2013;109:926–33.

[7] Suenaga M, Yamada S, Fujii T, *et al*. S-1 plus nab-paclitaxel is a promising regimen for pancreatic cancer in a preclinical model. J Surg Oncol 2016;113:413–9.

[8] Von Hoff DD, Ervin T, Arena FP, *et al*. Increased survival in pancreatic cancer with nab-paclitaxel plus gemcitabine. N Engl J Med 2013;369: 1691–703.

[9] Shi S, Liang C, Xu J, *et al*. The strain ratio as obtained by endoscopic ultrasonography elastography correlates with the stroma proportion and the prognosis of local pancreatic cancer. Ann Surg 2020;271:559–65.

[10] Hessmann E, Buchholz SM, Demir IE, *et al*. Microenvironmental determinants of pancreatic cancer. Physiol Rev 2020;100:1707–51.

[11] Klaassen R, Steins A, Gurney-Champion OJ, *et al*. Pathological validation and prognostic potential of quantitative MRI in the characterization of pancreas cancer: preliminary experience. Mol Oncol 2020;14: 2176–89.

[12] Meng Y, Zhang H, Li Q, *et al*. Magnetic resonance radiomics and machine-learning models: an approach for evaluating tumor-stroma ratio in patients with pancreatic ductal adenocarcinoma. Acad Radiol 2022; 29:523–35.

[13] Erstad DJ, Sojoodi M, Taylor MS, *et al*. Fibrotic response to neoadjuvant therapy predicts survival in pancreatic cancer and is measurable with collagen-targeted molecular MRI. Clin Cancer Res 2020;26:5007–18.

[14] Wegner CS, Gaustad JV, Andersen LM, *et al*. Diffusion-weighted and dynamic contrast-enhanced MRI of pancreatic adenocarcinoma xenografts: associations with tumor differentiation and collagen content. J Transl Med 2016;14:161.

[15] Nicolle R, Blum Y, Duconseil P, *et al*. Establishment of a pancreatic adenocarcinoma molecular gradient (PAMG) that predicts the clinical outcome of pancreatic cancer. EBioMedicine 2020;57:102858.

[16] Shi S, Luo Y, Wang M, *et al*. Tumor fibrosis correlates with the survival of patients with pancreatic adenocarcinoma and is predictable using clinicoradiological features. Eur Radiol 2022;32:6314–26.

[17] Fukui H, Onishi H, Nakamoto A, *et al*. Pancreatic fibrosis by extracellular volume fraction using Contrast-enhanced computed tomography and relationship with pancreatic cancer. Eur J Radiol 2022;156:110522.

[18] Wang Y, Chen ZE, Nikolaidis P, *et al*. Diffusion-weighted magnetic resonance imaging of pancreatic adenocarcinomas: association with histopathology and tumor grade. J Magn Reson Imaging 2011;33:136–42.

[19] Lambin P, Leijenaar RTH, Deist TM, *et al*. Radiomics: the bridge between medical imaging and personalized medicine. Nat Rev Clin Oncol 2017;14:749–62.

[20] Mukherjee S, Patra A, Khasawneh H, *et al*. Radiomics-based machine-learning models can detect pancreatic cancer on prediagnostic computed tomography scans at a substantial lead time before clinical diagnosis. Gastroenterology 2022;163:1435–46.e3.

[21] Do RKG, Kambadakone A. Radiomics for CT assessment of vascular contact in pancreatic adenocarcinoma. Radiology 2021;301:623–4.

[22] Li X, Wan Y, Lou J, *et al*. Preoperative recurrence prediction in pancreatic ductal adenocarcinoma after radical resection using radiomics of diagnostic computed tomography. eClinicalMedicine 2022;43:101215.

[23] Mathew G, Agha R, Albrecht J, *et al*. STROCSS 2021: Strengthening the Reporting of cohort, cross-sectional and case-control studies in Surgery. Int J Surg 2021;96:106165.

[24] Meng Y, Zhang H, Li Q, *et al*. CT radiomics and machine-learning models for predicting tumor-stroma ratio in patients with pancreatic ductal adenocarcinoma. Front Oncol 2021;11:707288.

[25] Xu S, Zhang XP, Zhao GD, *et al*. Derivation and validation of a preoperative prognostic model for resectable pancreatic ductal adenocarcinoma. Hepatob Pancreat Dis 2022;22:160–8.

[26] Liang Y, Sheng G, Guo Y, *et al*. Prognostic significance of grade of malignancy based on histopathological differentiation and Ki-67 in pancreatic ductal adenocarcinoma. Cancer Biol Med 2024;21:416–32.

[27] Schouten TJ, Kroon VJ, Besselink MG, *et al*. Perineural invasion is an important prognostic factor in patients with radically resected (R0) and node-negative (pN0) pancreatic cancer. Ann Surg 2024. [Online ahead of print].

[28] Perri G, Prakash L, Qiao W, *et al*. Postoperative chemotherapy benefits patients who received preoperative therapy and pancreatectomy for pancreatic adenocarcinoma. Ann Surg 2020;271:996–1002.

[29] Conzo G, Gambardella C, Tartaglia E, *et al*. Pancreatic fistula following pancreatoduodenectomy. Evaluation of different surgical approaches in the management of pancreatic stump. Literature review. Int J Surg 2015; 21(Suppl 1):S4–9.

[30] Mauriello C, Polistena A, Gambardella C, *et al*. Pancreatic stump closure after pancreatoduodenectomy in elderly patients: a retrospective clinical study. Aging Clin Exp Res 2016;29(Suppl 1):35–40.

[31] Adamska A, Domenichini A, Falasca M. Pancreatic ductal adenocarcinoma: current and evolving therapies. Int J Mol Sci 2017;18:1338.

[32] Chiou SH, Risca VI, Wang GX, *et al*. BLIMP1 induces transient metastatic heterogeneity in pancreatic cancer. Cancer Discov 2017;7: 1184–99.

[33] Lohse I, Lourenco C, Ibrahimov E, *et al*. Assessment of hypoxia in the stroma of patient-derived pancreatic tumor xenografts. Cancers (Basel) 2014;6:459–71.

[34] Drifka CR, Tod J, Loeffler AG, *et al*. Periductal stromal collagen topology of pancreatic ductal adenocarcinoma differs from that of normal and chronic pancreatitis. Modern Pathol 2015;28:1470–80.
[35] Drifka CR, Loeffler AG, Mathewson K, *et al*. Highly aligned stromal collagen is a negative prognostic factor following pancreatic ductal adenocarcinoma resection. Oncotarget 2016;7:76197–213.
[36] Sherman MH, Beatty GL. Tumor microenvironment in pancreatic cancer pathogenesis and therapeutic resistance. Annu Rev Pathol 2023;18:123–48.
[37] Andersen HB, Ialchina R, Pedersen SF, *et al*. Metabolic reprogramming by driver mutation-tumor microenvironment interplay in pancreatic cancer: new therapeutic targets. Cancer Metast Rev 2021;40:1093–114.
[38] Berenguer R, Pastor-Juan MDR, Canales-Vazquez J, *et al*. Radiomics of CT features may be nonreproducible and redundant: influence of CT acquisition parameters. Radiology 2018;288:407–15.
[39] Mackin D, Fave X, Zhang L, *et al*. Measuring computed tomography scanner variability of radiomics features. Invest Radiol 2015;50:757–65.
[40] Wu J, Li C, Gensheimer M, *et al*. Radiological tumor classification across imaging modality and histology. Nat Mach Intell 2021;3:787–98.
[41] Wottschel V, Alexander DC, Kwok PP, *et al*. Predicting outcome in clinically isolated syndrome using machine learning. Neuroimage Clin 2014;7:281–7.
[42] Wottschel V, Chard DT, Enzinger C, *et al*. SVM recursive feature elimination analyses of structural brain MRI predicts near-term relapses in patients with clinically isolated syndromes suggestive of multiple sclerosis. Neuroimage Clin 2019;24:102011.
[43] Teng X, Zhang J, Han X, *et al*. Explainable machine learning via intratumoral radiomics feature mapping for patient stratification in adjuvant chemotherapy for locoregionally advanced nasopharyngeal carcinoma. Radiol Med 2023;128:828–38.